Shear localization as a mesoscopic stress-relaxation mechanism in fused silica glass at high strain rates

W. Schill, J.P. Mendez, L. Stainier, M. Ortiz

PII: S0022-5096(20)30176-9
DOI: https://doi.org/10.1016/j.jmps.2020.103940
Reference: MPS 103940

To appear in: *Journal of the Mechanics and Physics of Solids*

Received date: 22 November 2019
Revised date: 12 March 2020
Accepted date: 14 March 2020

Please cite this article as: W. Schill, J.P. Mendez, L. Stainier, M. Ortiz, Shear localization as a mesoscopic stress-relaxation mechanism in fused silica glass at high strain rates, *Journal of the Mechanics and Physics of Solids* (2020), doi: https://doi.org/10.1016/j.jmps.2020.103940

SHEAR LOCALIZATION AS A MESOSCOPIC STRESS-RELAXATION MECHANISM IN FUSED SILICA GLASS AT HIGH STRAIN RATES

W. SCHILL[1], J. P. MENDEZ[1], L. STAINIER[2] AND M. ORTIZ[1]

Abstract. Molecular dynamics (MD) simulations of fused silica glass deforming in pressure-shear, while revealing useful insights into processes unfolding at the atomic level, fail spectacularly in that they grossly overestimate the magnitude of the stresses relative to those observed, e. g., in plate-impact experiments. We interpret this gap as evidence of relaxation mechanisms that operate at mesoscopic length-scales and which, therefore, are not taken into account in atomic-level calculations. We specifically hypothesize that the dominant mesoscopic relaxation mechanism is shear banding. We evaluate this hypothesis by first generating MD data over the relevant range of temperature and strain rate and then carrying out continuum shear-banding calculations in a plate-impact configuration using a critical-state plasticity model fitted to the MD data. The main outcome of the analysis is a knock-down factor due to shear banding that effectively brings the predicted level of stress into alignment with experimental observation, thus resolving the predictive gap of MD calculations.

1. Introduction

Fused silica glass is abundant in nature and is widely used as an engineering material in a number of areas of application, including protective armor. In a previous paper [1], we developed an atomistic model of fused silica glass and carried out molecular dynamics (MD) simulations aimed at interrogating the elastic and plastic behavior of the material over a wide range of pressures, cf. Fig. 1. The MD calculations faithfully capture the observed densification transition under volumetric compression and the permanent, or plastic, densification upon unloading. The MD data also reveals an evolution towards a critical state of constant volume under pressure-shear deformation, a behavior that is well-captured by a critical-state model of plasticity. Most remarkably, the MD data also captures the well-known anomalous non-monotonic pressure dependence of the shear modulus [2] and the observed non-convexity of the elastic domain in the pressure-shear plane [3]. The MD calculations additionally reveal insights into the mechanistic basis for these behaviors, including the occurrence of shear transformation zones (STZ) [4, 5], free-volume kinetics [6, 7, 8, 9], and changes in coordination number [10, 11, 12, 13, 14, 15].

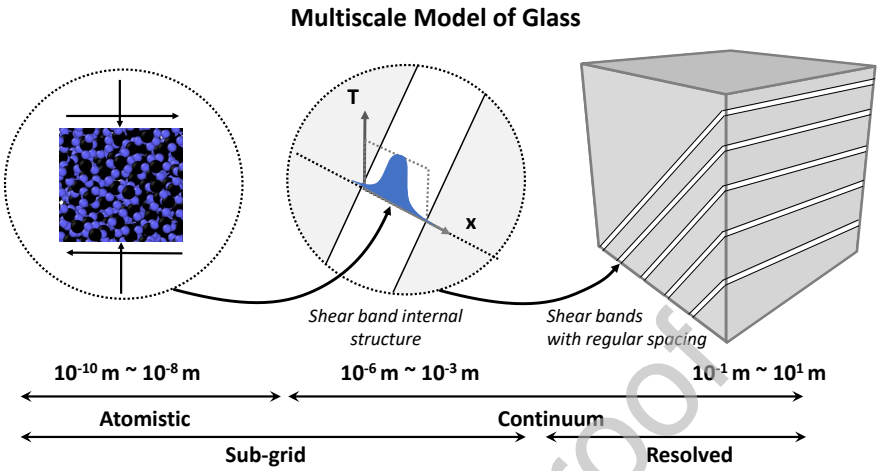

FIGURE 1. Schematic representation of the hypothesized multiscale hierarchy underlying the inelastic deformation of glass. Left: Atomistic scale encompasses shear transformation zones (STZ), free-volume kinetics and changes in atomic coordination number. Right: The macroscopic response depends critically on the operation of continuum relaxation mechanics such as shear banding. Center: The mesoscopic hand-shake occurs at the single-band scale and determines the shear-bank profile.

Despite these successes, MD calculations fail spectacularly in one important respect: they grossly overestimate the magnitude of the stresses relative to those observed, e. g., in plate-impact experiments [16, 17, 18, 19]. We interpret this gap as evidence of relaxation mechanisms that operate at mesoscopic lengthscales and which, therefore, are not taken into account in atomic-level calculations.

In the present work, we specifically hypothesize that the dominant relaxation mechanism is shear banding, cf. Fig. 1. Indeed, shear bands are commonly observed to form in amorphous systems such as metallic glasses under quasistatic loading [20, 21, 22] and in non-metallic glasses under dynamic loading [16, 17, 23]. In this latter case, shear banding may be expected to be nearly adiabatic. We evaluate the shear-banding hypothesis by extending the MD data mining of [1] for fused silica to include the dependence on temperature and strain rate over the relevant range and carrying out continuum shear-banding calculations in a plate-impact configuration. The main outcome of the analysis is a knock-down factor due to shear banding that effectively brings the predicted level of stress into alignment with experimental observation, thus closing the predictive gap of MD calculations.

2. Supporting Molecular Dynamic Calculations

In this section, we generate data describing silica glass by means of atomistic simulations. Specifically, we seek to ascertain the relationship between pressure, volume, shear stress, shear strain, temperature and shear-strain rate under conditions typical of impact loading.

2.1. **Temperature.** The model used in calculations has been described in [1]. We consider a sample of 1536 atom fused-silica initial configurations obtained by a melt-quench procedure beginning from a β-crystobolite. We utilize a Nosé-Hoover (NPT) barostat to control the pressure and temperature and the applied strain rate is of the order of 10^8 1/s. To account for the effect of variation in amorphous atomic structure, four different initial conditions are prepared. The differences between the initial conditions is introduced during the melt-quench procedure by running the melting stage for different lengths of time (see [1]). All the results in this section are obtained by computing an average over the resulting trajectories.

We first study the effect of temperature on densification and shear behavior of silica glass. In Fig. 2, we display pressure versus consolidation for a large range of temperatures from $300K$ up to $1900K$. Independently of temperature, the material exhibits extensive consolidation as evidenced by the unloading curves and a distinctive increase in slope during loading.

We may gain insight from the molecular dynamics calculations into the underlying physics in this regime. The low density phase of silica, which is 4-fold coordinated (see Fig. 3), has a volume which is nearly independent of temperature. The equilibrium volume of the high density phase of silica, which is 6-fold coordinated, has substantial dependence on temperature. An alternative hypothesis is that the tradeoff between 6-fold and 5-fold coordinated symmetry in the high density phase of silica becomes reversible at high temperature due to thermal activation, thereby resulting in a reduction in permanent consolidation.

2.2. **Pressure-shear deformation.** We now examine the effect of combined volumetric and shear deformation. In Fig. 4, we display shear stress *vs.* shear strain for several temperatures. The behavior is qualitatively consistent across a wide range of temperatures, exhibiting an elastic region and plastic region. In each case, for a given shear strain, the shear stress first decreases with increasing pressure and then increases. Furthermore, as the temperature increases, the stress decreases.

The inelastic shear deformation is accommodated by *Shear transformation zones*(STZ) (c.f. [1, 24]). An STZ is a localized highly non-affine rearrangement of atomic positions. The stress-strain trajectories are characterized by a saw-tooth behavior where the stress drops whenever a STZ occurs.

Additionally, the shear yield stress profile in silica exhibits an anomalous dependence on the pressure ([1]). In particular, this is accommodated at the

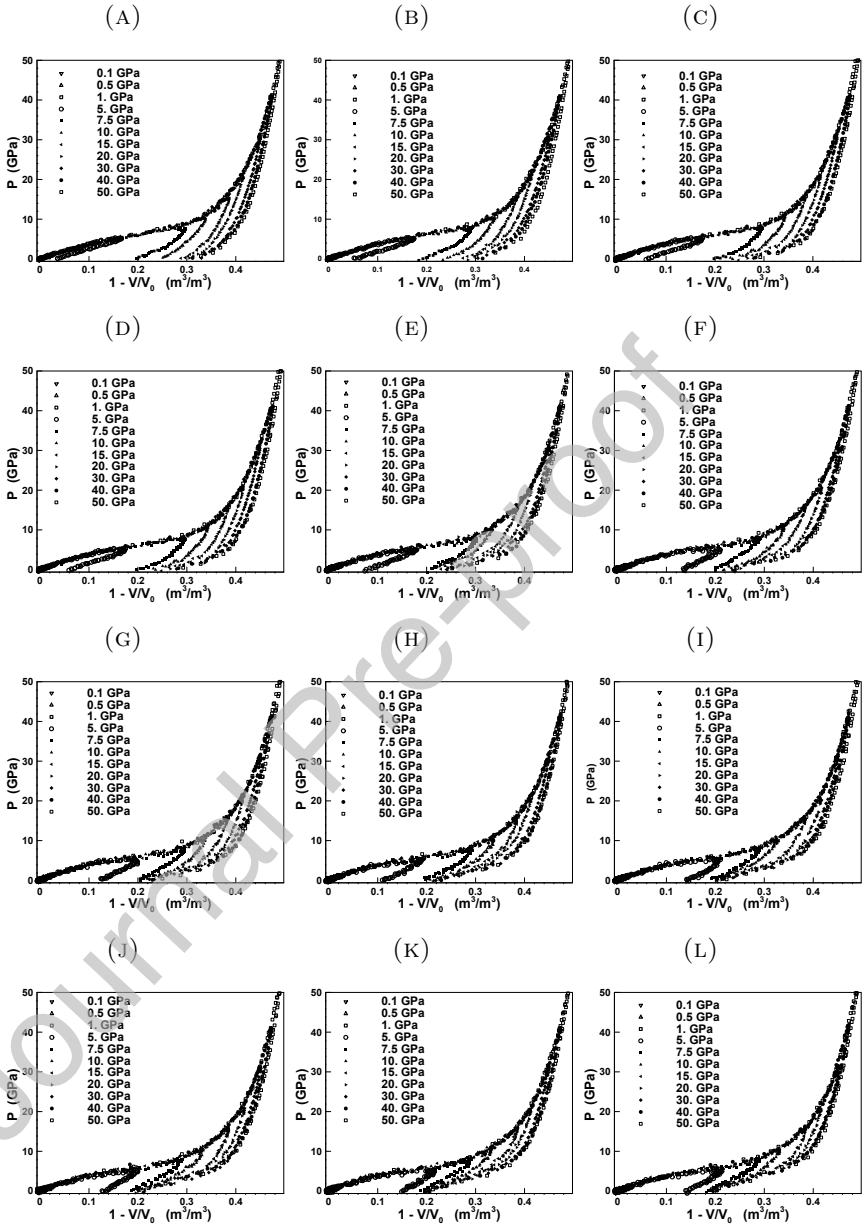

FIGURE 2. The isothermal pressure-compression relationship at temperatures T = (a) 400 (b) 600; (c) 800 (d) 1000 (e) 1200 (f) 1300 (g)1400 (h) 1500 (i) 1600 (j) 1700(k) 1800 (l) 1900 K.

microstructural level through the formation of microstress patterns. This pattern formation may be viewed from the perspective of relaxation theory. A related theory for micromechanical mechanism in amorphous solids

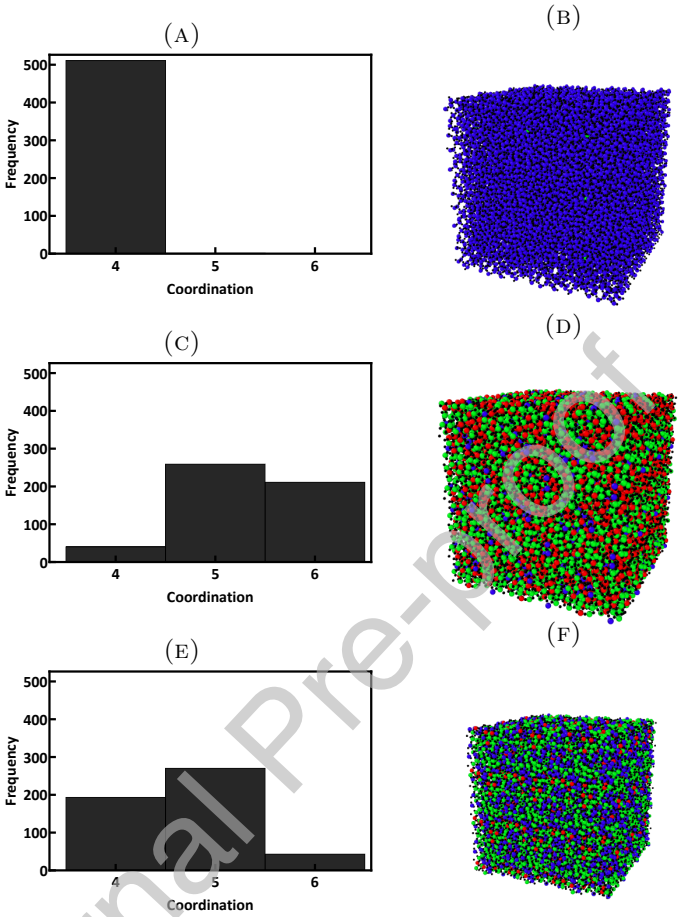

FIGURE 3. We display the coordination number at 1900 K.

is *free volume kinetics*. Such theories have been applied to model plastic deformation in [22].

2.3. **Rate of deformation.**

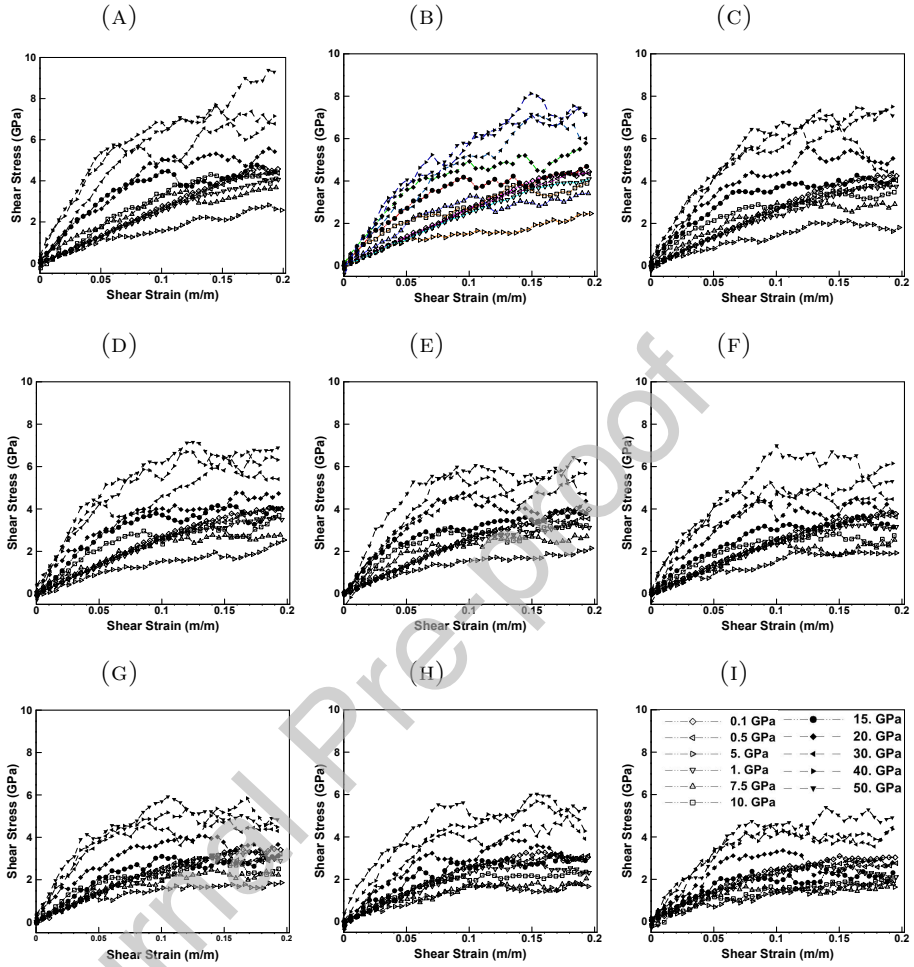

FIGURE 4. The shear stress-shear strain relation at temperatures T = (a) 400 (b) 500; (c) 700 (d) 900 (e) 1100 (f) 1300 (g)1500 (h) 1700 (i) 1900 K. The legend included in (i) applies to all the figures.

Next, we investigate the effect of strain rate on the behavior silica glass over a range of strains from 10^7 to 10^{10} 1/s. A difficulty that arises in this pursuit is that low strain rates are outside the range of applicability of molecular dynamics. We overcome this difficulty by recourse to maximum-entropy (max-ent) non-equilibrium statistical mechanics. In addition, atomic-scale inertia is known to be negligible at low strain rates [25]. We therefore run the low strain rate max-ent calculations in quasistatic mode using an implementation of MaxEnt-Lammps due to Ponga *et al.* [26]. Detailed accounts of the max-ent method may be found in [27, 28, 29, 30] and references therein.

Fig. 5 displays rate-dependence curves computed using standard molecular dynamics at high strain rates and max-ent quasistatics at low strain rate, including the effect of temperature. The general trend observed in the figure is that the stress decreases as a function of decreasing strain rate. In addition, the rate of loading has minimal effect for low temperatures 300K. However, this decrease becomes more pronounced at increasing temperatures and pressures.

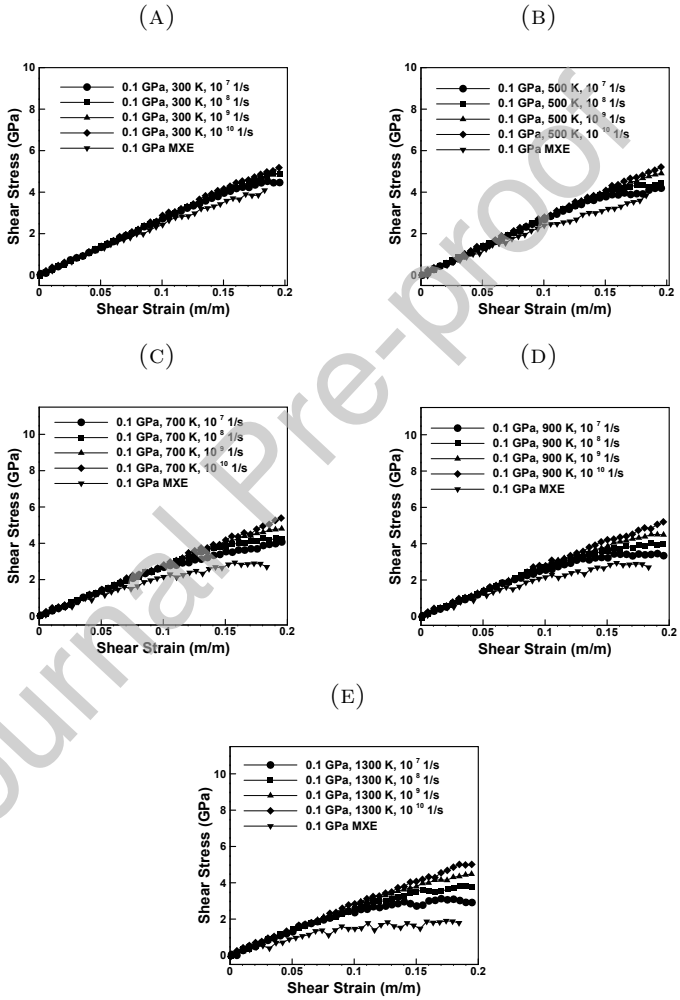

(F)

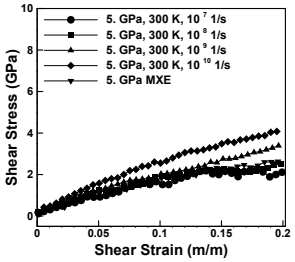

(G)

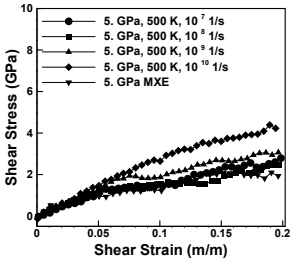

(H)

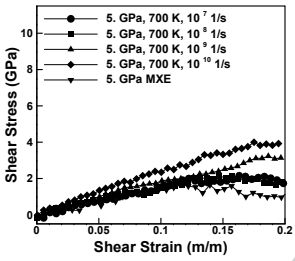

(I)

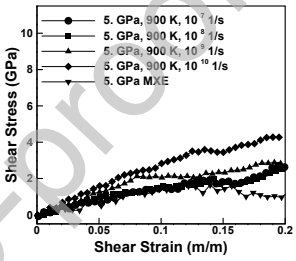

(J)

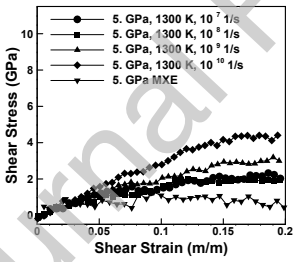

(K)

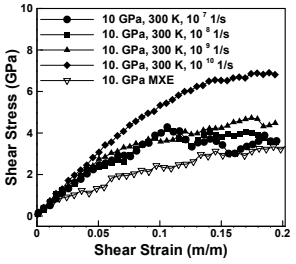

(L)

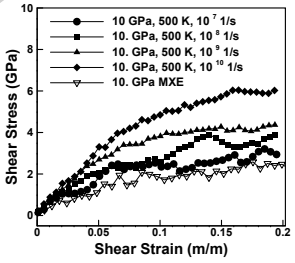

(M)

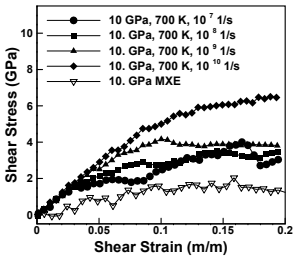

(N)

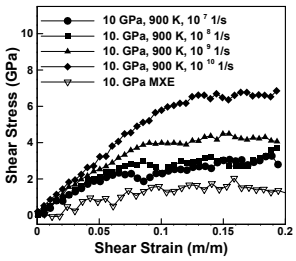

(O)

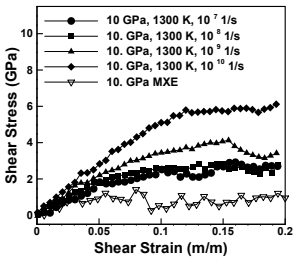

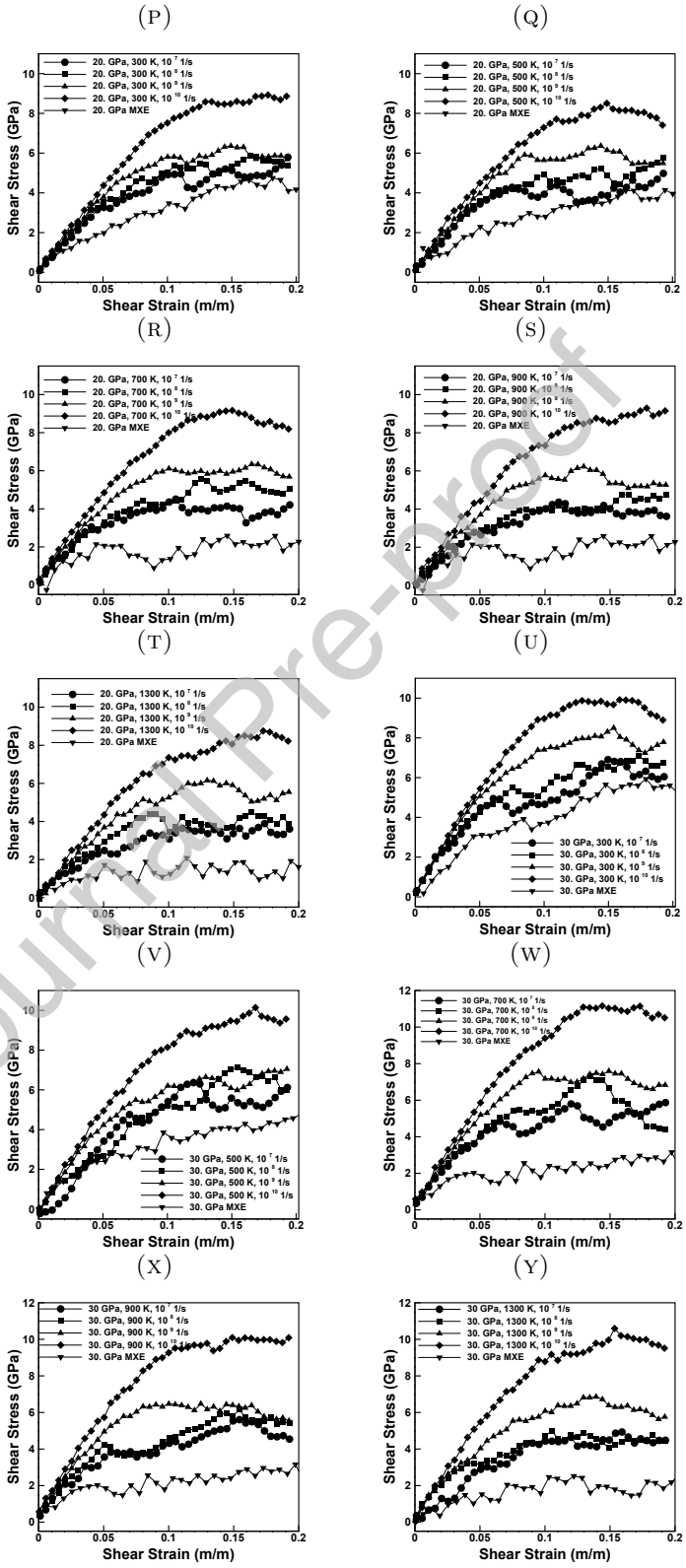

FIGURE 5. The shear strain rate behavior at various temperatures and pressures. The calculated stress strain relations are shown for pressures of $p = 0.1$ GPa, 5 GPa, 10 GPa , 20 GPa, and 30 GPa for several temperatures and strain rates.

3. Continuum model

With a view to the shear-banding analyses that follow, we proceed to modify the constitutive model recently introduced by [1] to incorporate temperature and rate dependency. We assume a free energy of the form

$$A(F,F^p,T)=\frac{\mu(J^e,T)}{2}\Big(J^{e-2/3}\,\mathrm{tr}(C^e)-3\Big)+f(J^e,T). \tag{1}$$

Cam-Clay yield criterion,

$$\left(\frac{2p-p_c-p_t}{p_c-p_t}\right)^2+\left(\frac{q}{q_c}\right)^2=1. \tag{2}$$

In the rate-independent limit, hardening is determined by the locus of points (p_m,q_c), $p_m=(p_c-p_t)/2$, in the (p,q)-plane, or critical state line, and the consolidation relation $p_c(J^p)$. We assume a reference critical state line of the form

$$q_c(p_m,T=T_0,\dot\gamma=\dot\gamma_0)=\begin{cases}\dfrac{p_1-p_m}{p_1-p_t}\,q_t, & p_m\le p_1,\\ \Big(s+\frac{3}{4}(p_m-r)^2\Big)^{1/2}, & p_1\le p_m\le p_2,\\ Bp^\beta, & p_2\le p_m.\end{cases} \tag{3}$$

We recall [1] that a critical state line of this form is the correct macroscopic limit resulting from microscopic stress field fluctuations. In general, the effective shear stress q_c at the critical state depends on temperature and strain rate, cf. Sections 2.2 and 2.3. We account for this dependence through a critical-state line of the power-law form

$$\begin{aligned}&q_c(p_m,T,\dot\gamma)=\\ &q_c(p_m,T=T_0,\dot\gamma=\dot\gamma_0)\,c_1\left(\gamma_0\dot\gamma^{m_1+m_2T}+1\right)\left(\frac{T}{T_0}\right)^{\nu_2\log(\dot\gamma)+\nu_1}\end{aligned}, \tag{4}$$

and a consolidation relation of the form

$$\begin{aligned}p_c(J^p,T)&=\frac{J^p}{J}\frac{\partial W^p}{\partial J^p}\\ &=p_0+\frac{A_0}{\alpha}(1-J^{p-\alpha})+A_1\exp\Big(\frac{m_0(J_c-J_p)(T-T_0)}{J_c}\Big)\end{aligned}, \tag{5}$$

where A_1, A_0 are fitted to the MD consolidation curves at different temperatures. The parameters are provided in tables 1, 2, and 3. Further details and additional parameters, including the assumed form of the elasticity functions μ and f may be found in [31].

Table 1. Critical state line constants

q_t	p_t	B	β
7.402 GPa	−8.5 GPa	1.168 $\sqrt{\text{GPa}}$	0.5

TABLE 2. Critical state line constants specific to rank two connection

p_1	p_2	r	s
4.141 GPa	6.084 GPa	5.176 GPa	7.674 GPa^2

TABLE 3. Thermal and shear rate critical state line parameters.

ν_1	m_1	ν_2	m_2	γ_0	c_1
-0.70	0.462	0.0288	5.26×10^{-6}	0.0000141	0.942

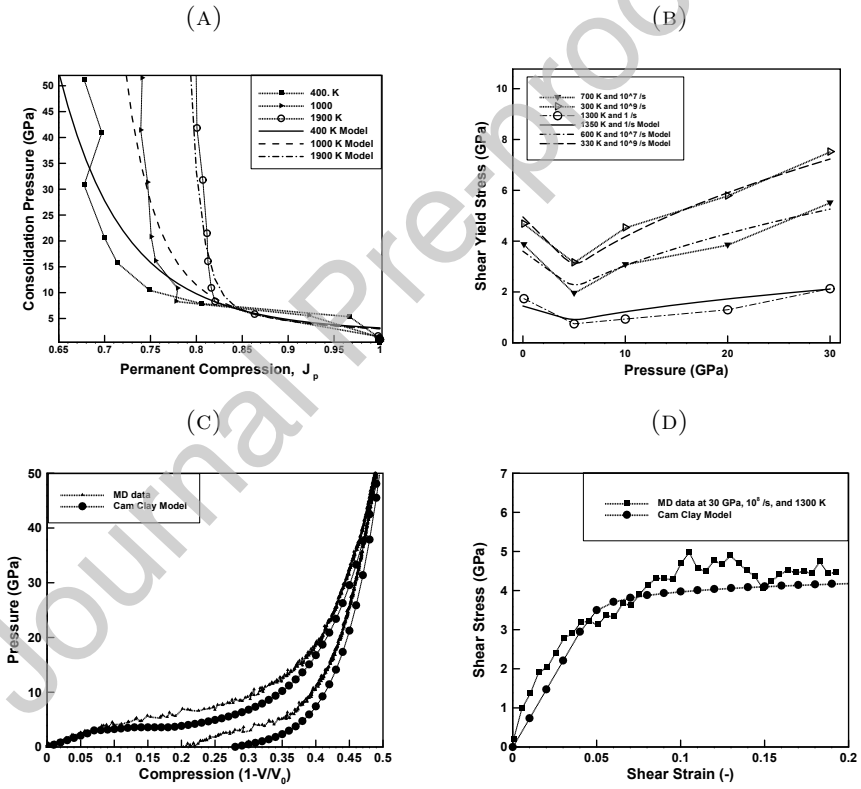

FIGURE 6. Selected comparisons with MD data illustrating the goodness of fit achieved by the continuum model. a) Pressure consolidation relation. b) Shear yield stress *v.* pressure and strain rate. c) Pressure-volume response. d) Pressure-shear response.

Fig. 6 displays selected comparisons with the MD data that illustrate the goodness of fit achieved by the critical-state continuum model. The model

reproduces salient aspects of the MD data, including the densification transition at around 5 GPa and the permanent or plastic densification upon unloading, the pressure-shear response, including shear-induced densification and hardening (loosening and softening) at low (hight) preconsolidation, the anomalous non-convex dependence of the shear strength on pressure and the dependence on temperature and strain rate. In bear emphasis that the non-convexity of the elastic domain in the pressure-shear plane, is consistent with that identified by [1] and persists over a broad range of strain rates and temperatures. We refer the reader to [31] for additional examples.

4. Localization analysis

As noted in the introduction, the MD data just reported, and the continuum model fitted to those data, grossly overestimate the level of stress measured experimental, e. g., in plate-impact experiments [16, 17, 18, 19], whence we conclude that there must be additional relaxation mechanisms at the mesoscale that bring the stresses down to the level of observation. Remarkably, we note from Table 3 that $m + \nu < 0$, which suggests that fused silica glass is prone to adiabatic shear localization [32]. We proceed to analyze the efficiency of adiabatic shear localization as a relaxation mechanism and its ability to close the gap between atomic-level predictions and observation. For definiteness and to facilitate comparisons with experiment, we confine attention to deformations corresponding to pressure-shear plate-impact tests [16, 17, 18, 19].

4.1. **Steady state analysis.** We consider a plate in a state of pressure-shear stress

$$\sigma(x) = \begin{pmatrix} \sigma_{11}(x_3) & 0 & \sigma_{13}(x_3) \\ 0 & \sigma_{22}(x_3) & 0 \\ \sigma_{31}(x_3) & 0 & \sigma_{33}(x_3) \end{pmatrix}. \tag{6}$$

where (x_1, x_2) is the plane of the plate and x_3 the transverse direction. Static equilibrium demands,

$$\sigma'_{13}(x_3) = 0, \qquad \sigma'_{33}(x_3) = 0, \tag{7}$$

whence in follows that $\sigma_{13}(x_3)$ and $\sigma_{33}(x_3)$ are constant and no equilibrium restrictions apply to $\sigma_{11}(x_3)$ and $\sigma_{22}(x_3)$. In addition, we assume that at steady state the entire plate is critical and undergoes pure shear,

$$d(x_3) = d^p(x_3) = \begin{pmatrix} 0 & 0 & d_{13}(x_3) \\ 0 & 0 & 0 \\ d_{31}(x_3) & 0 & 0 \end{pmatrix}, \tag{8}$$

where $d(x_3)$ is the rate-of-deformation tensor and d^p is its plastic component. From the flow rule, at the critical state we have,

$$d^p(x) \propto s(x) \ , \tag{9}$$

where $s(x)$ denotes the stress deviator. From these relations, we conclude

$$\sigma_{11}(x_3) = \sigma_{22}(x_3) = \sigma_{33}(x_3) = p = \text{constant}. \tag{10}$$

Inverting equation (4), we obtain the relation

$$\dot{\gamma}(z) = f(p, \tau, T(z)). \tag{11}$$

where we write $z = x_3$, $\dot{\gamma} = 2d_{13}$ and $\tau = \sigma_{13}$ for shorthand.

Under the conditions of the analysis, the heat equation reduces to the one-dimensional form

$$\rho c T_{,t}\,(z,t) = \kappa T_{,zz}\,(z,t) + \tau\dot{\gamma}(z,t), \tag{12}$$

where, for simplicity, we assume that all plastic work is converted to heat. Inserting relation (11) into this equation, we obtain

$$\rho c T_{,t}\,(z,t) = \kappa T_{,zz}\,(z,t) + \tau f(p, \tau, T(z,t)). \tag{13}$$

We additionally append velocity boundary conditions of the form

$$\int_0^L \dot{\gamma}(z,t)\,dz = v, \tag{14}$$

where L is the thickness of the plate and v is the prescribed velocity, and adiabatic boundary conditions,

$$\kappa T_{,z}\,(0,t) = \kappa T_{,z}\,(L,t) = 0. \tag{15}$$

At steady state, (12) reduces to

$$\kappa T_{,zz}\,(z) + \tau f(p, \tau, T(z)) = 0. \tag{16}$$

This is the Euler-Lagrange equation of the minimum problem

$$F(T) = \int_0^L \Big(\frac{\kappa}{2} T_{,z}^{\,2}\,(z) + g(T(z))\Big)\,dz \to \min!, \tag{17}$$

with

$$g'(T) = -\tau f(p, \tau, T), \tag{18}$$

which renders the problem in variational form.

For materials prone to adiabatic shear localization, we expect the solution to localize into shear bands having an optimal profile in the sense of (17). The optimal profile can be determined analytically using a trick of Kohn and Müller [33, 34]. Multiply (16) by $T_{,z}\,(z)$ to obtain

$$-\kappa T_{,zz}\,(z) T_{,z}\,(z) + g'(T(z)) T_{,z}\,(z) = 0, \tag{19}$$

or

$$\frac{d}{dz}\Big(- \kappa T_{,z}^{\,2}\,(z) + g(T(z))\Big) = 0. \tag{20}$$

Integrating,

$$-\frac{\kappa}{2} T_{,z}^{\,2}\,(z) + g(T(z)) = C, \tag{21}$$

where C is a constant of integration. Suppose that the edge of the of shear band is at z_A and the mid point at z_M. By symmetry at the middle we have $T_{,z}(z_M) = 0$, whence $C = g(T(z_M))$ and

$$\frac{\kappa}{2} T_{,z}^{2}(z) = g(T(z)) - g(T(z_M)), \tag{22}$$

which is a statement of equipartition of dissipation. The total dissipation across one interface can now be computed as

$$\begin{aligned} F_{\text{int}} &= \int_{z_A}^{z_M} \Big(\frac{\kappa}{2} T_{,z}^{2}(z) + g(T(z)) \Big)\, dz \\ &= \int_{z_A}^{z_M} 2g(T(z)) - g(T_M)\, dz \\ &= \int_{T_A}^{T_M} \sqrt{2\kappa \big(g(T) - g(T_M) \big)}\, dT + h g(T_M) \ , \end{aligned} \tag{23}$$

where $T_A = T(z_A)$, $T_M = T(z_M)$ and h is the thickness of the interface. The thickness of the interface follows from (22) as

$$h = z_M - z_A = \int_{T_A}^{T_M} \sqrt{\frac{\kappa}{2\big(g(T) - g(T_M)\big)}}\, dT \ . \tag{24}$$

We may solve equations (24) and (14) numerically for τ and T_M for given v and h. Subsequently, the temperature profile follows from (22), which is separable and can be solved explicitly up to a quadrature, and the shear strain rate profile follows from (11).

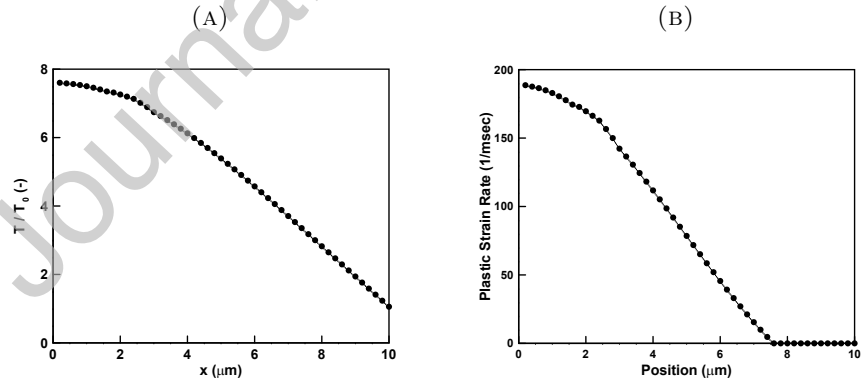

FIGURE 7. Optimal profile of shear band in fused-silica glass at pressure $p = 0$ GPa, applied shear $\tau = 0.44\ q_c(p)$ and initial temperature $T_0 = 300$K. a) Temperature profile; b) Shear strain rate.

Sample temperature and strain-rate profiles for pressure $p = 0$ GPa, applied shear $\tau = 0.44\ q_c(p)$ and initial temperature $T_0 = 300$K are shown in Fig. 7. The temperature in the shear band rises sharply above the ambient

temperature and peaks at the center of the shear band, as expected. The deformation vanishes outside the shear band, which moves rigidly at the prescribed velocity, and attains a maximum value of $2 \times 10^5 1/s$ at the center of the band. Interestingly, due to the cusp in the dissipation potential at the origin, the shear strain rate exhibits a slope discontinuity at the boundary of the shear band as it decreases to zero.

The preceding results bear out the hypothesis that fuse silica glass becomes unstable and undergoes adiabatic shear banding at sufficiently high strain rates characteristic of dynamic impact loading.

4.2. **Comparison with pressure-shear impact experiments.** It remains to be verified that shear banding results in stress levels consistent with observation. To this end, we aim to replicate the conditions of the plane-impact experiment of Clifton *et al.* [16, 17, 18, 19] at steady state. Pressure-shear experiments are designed to subject specimens to well-characterized, easy to interpret, states of stress and deformation with compressive stresses on glass specimens of the order of 3 GPa and shear strain rates of the order of 10^5 1/s.

The response of soda-lime glasses and similar glasses to impact loading has received considerable attention owing to the observation of failure waves [35, 36, 37, 38, 39, 40, 16]. When the glasses are subjected to normal impact above a certain threshold compressive stress, a failure front is observed to move from the impact face at a speed of approximately one-third the longitudinal wave speed of the intact glass. The measurements are generally interpreted as an indication that the glass behind the failure front possesses lower impedance, corresponding to a fall in shear strength, than the intact material.

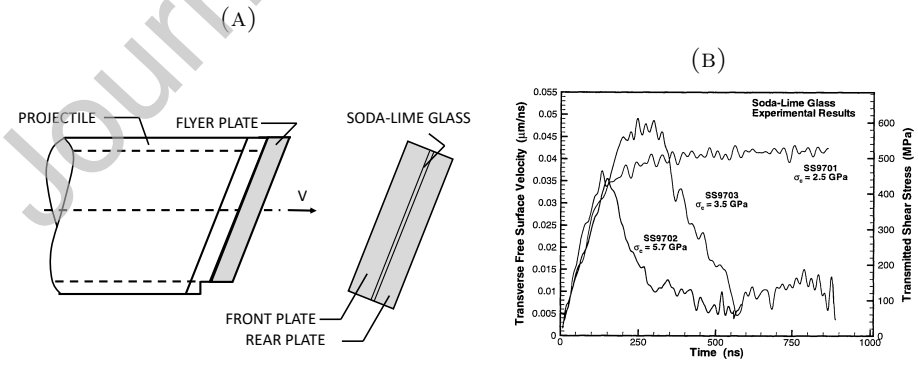

FIGURE 8. Pressure-shear plate impact experiments of soda lime glass [41, 23]. a) Experimental setup. b) Shear stress evolution for three different shots.

TABLE 4. Soda lime glass pressure-shear plate impact experiments of Sundaram and Clifton [41, 23].

Shot No.	Skew angle (degrees)	Projectile velocity (mm/μs)	Shear strain rate (1/s)	Compressive stress (GPa)	Shear stress (MPa)
SS9701	22	0.118	0.5×10^6	2.5	510
SS9703	22	0.169	3.2×10^6	3.5	100
SS9702	22	0.198	NA	5.7	60

Sundaram and Clifton [41, 23] tested soda lime glass, commonly referred to as *plate glass* or *window glass*, in a pressure-shear plate impact sandwich configuration. In these experiments, a flyer plate travelling at speeds of the order of 50-500 m/s strikes a stationary target plate, Fig. 8a. Stress waves generated upon impact travel through the target plate and are monitored at the rear surface using laser interferometry. In pressure-shear impact experiments the impacting plates are inclined relative to their direction of approach, which results in compressive as well as shear waves. The targets consist of a thin specimen film (5-500 μm) sandwiched between two thick elastic plates, causing the specimen film to undergo extremely high shearing rates. Since the plates remain elastic during the experiment, one-dimensional elastic stress wave theory can be used to obtain the stresses and nominal strain rates in the specimen from the recorded rear-surface motion.

Sundaram and Clifton [41, 23] carried out three high strain-rate pressure-shear plate impact experiments on the soda-lime glass. Table 4 summarizes the parameters for the three shots and Fig. 8b shows the measured transverse velocity/shear stress profiles after the first arrival of the transmitted shear wave. For the low-velocity shot (SS9701), the normal compressive stress on the soda-lime glass is 2.5 GPa and the shear stress saturates at 510 MPa with no apparent loss of bearing capacity. By contrast, for the high-velocity shots (SS9703 and SS9702) the normal compressive stress rises to 3.5 GPa and 5.7 GPa, respectively, and the shear stress dramatically falls to values of approximately 100 MPa and 60 MPa, respectively, after an initial ramping increase.

Table 5 collects the results of steady-state shear-banding calculations for the normal compressive stress and average shear-strain rate corresponding to the three shots reported by Sundaram and Clifton [41, 23]. For comparison, Table 5 also collects the values reported by Sundaram and Clifton [41, 23] at steady state and the values computed without shear banding, i. e., under uniform deformation conditions. As may be seen from the table, the uniform-deformation shear stresses greatly overestimate the experimental values. The large knock-down factor in shear stress induced by shear banding is quite remarkable and brings the computed shear stresses into

TABLE 5. Comparison of steady-state values computed from shear-banding analysis and pressure-shear plate impact experiments of Sundaram and Clifton [41, 23].

Shot No.	Shear stress (experiment) (MPa)	Shear stress (uniform) (MPa)	Shear stress (shear banding) (MPa)	Peak temperature (K)	Shear band thickness (μm)
SS9701	510	2410.38	600.249	2186.52	12.3542
SS9703	100–180	624.288	155.094	2193.95	22.9908
SS9702	60–80	396.289	98.4295	2194.54	34.5278

alignment with the experimental measurements. This agreement is specially remarkable considering that the data corresponds to soda-lime glass whereas the model calculations correspond to fused silica, which suggests that the behavior of both glasses is quite similar.

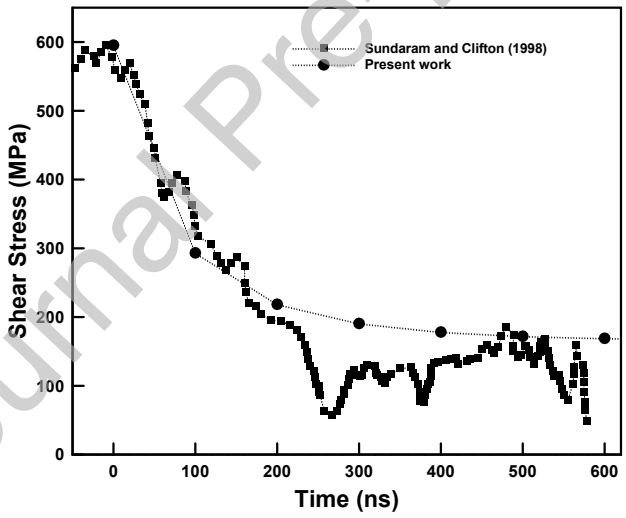

FIGURE 9. Comparison of the computed transient shear-banding shear stress *vs.* time for shot SS9703 and the experimental data of Sundaram and Clifton [23] after the end of the initial ramp.

Fig. 9 shows a comparison of the computed transient shear-banding shear stress *vs.* time for shot SS9703 and the experimental data after the end of the initial ramp. The agreement between the calculated and measured shear stresses is likewise remarkable and, again, suggests that the behavior of soda-lime glass and fused silica is quite similar.

5. Summary and concluding remarks

Molecular dynamics (MD) simulations of fused silica glass deforming in pressure-shear, while revealing useful insights into processes unfolding at the atomic level, fail spectacularly in that they grossly overestimate the magnitude of the stresses relative to those observed, e. g., in plate-impact experiments. We interpret this gap as evidence of relaxation mechanisms that operate at mesoscopic lengthscales and which, therefore, are not taken into account in atomic-level calculations. We specifically hypothesize that the dominant mesoscopic relaxation mechanism is shear banding. We have evaluated this hypothesis by first generating MD data over the relevant range of temperature and strain rate and then carrying out continuum shear-banding calculations in a plate-impact configuration using a critical-state plasticity model fitted to the MD data. The main outcome of the analysis is a knock-down factor due to shear banding that effectively brings the predicted level of stress into alignment with experimental observation, thus resolving the predictive gap of MD calculations.

The failure of MD to predict levels of stress in fused silica glass consistent with observation provides a noteworthy cautionary tale on the limitations of MD calculations. As noted by Ortiz *et al.* [42], while many of the fundamental mechanisms underlying the inelastic behavior of materials are mediated by crystal-lattice defects and are, therefore, accessible to direct atomistic simulation, either by means of empirical potentials or through *ab initio* quantum-mechanical calculations, the relevance of atomistic calculations as regards the macroscopic behavior of materials is often overstated. To be sure, there are macroscopic phenomena which can be directly elucidated at the atomic scale, e. g., first-principles calculations of the equation of state (EoS) and the elastic moduli of metals up to high pressures and temperatures. However, in general atomic-scale mechanisms are separated from the macroscopic behavior they underlie by a vast array of intervening *continuum scales*. These mesoscopic scales both filter (average) and modulate (set the boundary conditions or driving forces for) the atomic-scale phenomena and are an essential part of the understanding of material behavior. This realization takes on special significance due to overwhelming dominance of MD calculations in present-day materials research.

Acknowledgements

We gratefully acknowledge support from the US Office of Naval Research, Naval Materials S&T Division, Dr. R. G. Barsoum manager, through grant N000141512453. This work was supported by a NASA Space Technology Research Fellowship. We are also grateful to R. J. Clifton for many illuminating comments and suggestions.

References

[1] W. Schill, S. Heyden, S. Conti, and M. Ortiz. The anomalous yield behavior of fused silica glass. *Journal of the Mechanics and Physics of Solids*, 113:105 – 125, 2018.

[2] K. Kondo, S. Iio, and A. Sawaoka. Nonlinear pressure dependence of the elastic moduli of fused quartz up to 3 GPa. *Journal of Applied Physics*, 52(4):2826–2831, 1981.

[3] C. Meade and R. Jeanloz. Effect of a coordination change on the strength of amorphous SiO_2. *Science*, 241(4869):1072–1074, 1988.

[4] M. L. Falk and J. S. Langer. Dynamics of viscoplastic deformation in amorphous solids. *Phys. Rev. E*, 57:7192–7205, Jun 1998.

[5] J. S. Langer. Microstructural shear localization in plastic deformation of amorphous solids. *Phys. Rev. E*, 64:011504, Jun 2001.

[6] M. H. Chen and M. Goldstein. Anomalous viscoelastic behavior of metallic glasses of Pd-Si-based alloys. *Journal of Applied Physics*, 43(4):1642–1648, 1972.

[7] D. E. Polk and D. Turnbull. Flow of melt and glass forms of metallic alloys. *Acta Metallurgica*, 20(4):493–498, 1972.

[8] F. Spaepen. A microscopic mechanism for steady state inhomogeneous flow in metallic glasses. *Acta Metallurgica*, 25(4):407–415, 1977.

[9] A. S. Argon. Plastic deformation in metallic glasses. *Acta Metallurgica*, 27(1):47–58, 1979.

[10] T. Sato and N. Funamori. High-pressure structural transformation of SiO_2 glass up to 100 GPa. *Phys. Rev. B*, 82:184102, Nov 2010.

[11] T. Sato and N. Funamori. Sixfold-coordinated amorphous polymorph of SiO_2 under high pressure. *Phys. Rev. Lett.*, 101:255502, Dec 2008.

[12] D. Wakabayashi, N. Funamori, T. Sato, and T. Taniguchi. Compression behavior of densified SiO_2 glass. *Phys. Rev. B*, 84:144103, Oct 2011.

[13] D. Vandembroucq, T. Deschamps, C. Coussa, A. Perriot, E. Barthel, B. Champagnon, and C. Martinet. Density hardening plasticity and mechanical ageing of silica glass under pressure: a raman spectroscopic study. *Journal of Physics: Condensed Matter*, 20(48):485221, 2008.

[14] Y. Inamura, Y. Katayama, W. Utsumi, and K.-I. Funakoshi. Transformations in the Intermediate-Range Structure of SiO_2 Glass under High Pressure and Temperature. *Physical Review Letters*, 93(1):015501, June 2004.

[15] S. N. Luo, O. Tschaune, P. D. Asimow, and T. J. Ahrens. A new dense silica polymorph: A possible link between tetrahedrally and octahedrally coordinated silica. *American Mineralogist*, 89:455461, 2004.

[16] R. J. Clifton, M. Mello, and N. S. Brar. Effect of shear on failure waves in soda lime glass. *AIP Conference Proceedings*, 429(1):521–524, 1998.

[17] A. S. AbouSayed and R. J. Clifton. Pressure shear waves in fused silica. *Journal of Applied Physics*, 47(5):1762–1770, 1976.

[18] S. Sundaram and R. J. Clifton. Flow behavior of soda-lime glass at high pressures and high shear rates. In *American Institute of Physics Conference Series*, volume 429 of *American Institute of Physics Conference Series*, pages 517–520, July 1998.

[19] C. H. M. Simha and Y. M. Gupta. Time-dependent inelastic deformation of shocked soda-lime glass. *Journal of Applied Physics*, 96(4):1880–1890, 2004.

[20] R. D. Conner, W. L. Johnson, N. E. Paton, and W. D. Nix. Shear bands and cracking of metallic glass in bending. *Journal of Applied Physics*, 94:904-911, 2003.

[21] R. D. Conner, A. J. Rosakis, W. L. Johnson, and D. M. Owen. Fracture toughness determination for a beryllium-bearing bulk metallic glass. *Scripta Mater.*, 37:1373-1378, 1997.

[22] Q. Yang, A. Mota and M. Ortiz. A finite-deformation constitutive model of bulk metallic glass plasticity. *Computational Mechanics*, 37(2):194–204, 2006.

[23] S. Sundaram and R. J. Clifton. Flow behavior of soda-lime glass at high pressures and high shear rates. In *American Institute of Physics Conference Series*, volume 429 of *American Institute of Physics Conference Series*, pages 517–520, July 1998.
[24] M. L. Falk and J. S. Langer. Dynamics of viscoplastic deformation in amorphous solids. *Physical Review E*, 57(6):7192, 1998.
[25] E. B. Tadmor and R. E. Miller. *Modeling materials: continuum, atomistic and multiscale techniques*. Cambridge University Press, 2011.
[26] J. P. Mendez and M. Ponga. MXE: A package for simulating long-term diffusive mass transport phenomena in nanoscale systems. arXiv preprint arXiv:1910.01235, 2019.
[27] M. P. Ariza, I. Romero, M. Ponga and M. Ortiz. HotQC simulation of nanovoid growth under tension in copper. *International journal of fracture*, 174(1):75–85, 2012.
[28] Y. Kulkarni, J. Knap and M. Ortiz. A variational approach to coarse graining of equilibrium and non-equilibrium atomistic description at finite temperature. *Journal of the Mechanics and Physics of Solids*, 56(4):1417–1449, 2008.
[29] J. Marian, G. Venturini, B. L. Hansen, J. Knap, M. Ortiz and G. H. Campbell. Finite-temperature extension of the quasicontinuum method using Langevin dynamics: entropy losses and analysis of errors. *Modelling and Simulation in Materials Science and Engineering*, 18(1):015003, 2009.
[30] G. Venturini, K. Wang, I. Romero, M. P. Ariza and M. Ortiz. Atomistic long-term simulation of heat and mass transport. *Journal of the Mechanics and Physics of Solids*, 73:242–268, 2014.
[31] W. Schill. *Variational and multiscale modeling of amorphous silica glass*. Ph. D. Dissertation, Caltech, 2019.
[32] A. Molinari and R. J. Clifton. Analytical characterization of shear localization in thermoviscoplastic materials. *Journal of Applied Mechanics*, 54(4):806–812, 1987.
[33] R. V. Kohn and S. Müller. Relaxation and regularization of nonconvex variational problems. *Rendiconti del Seminario Matematico e Fisico di Milano*, 62(1):89–113, 1992.
[34] Y. Bai and B. Dodd. *Adiabatic shear localization: occurrence, theories, and applications*. Pergamon Press, 1992.
[35] G. I. Kanel, S. V. Rasorenov and V. E. Fortov. The failure waves and spallations in homogeneous brittle materials. In J. W. Forbes S. C. Schmidt, R. D. Dick and D. G. Tasker, editors, *Shock Compression of Condensed Matter*, Proceedings of the American Physical Society Topical Conference Held in Williamsburg, Virginia, June 1720, 1991, pages 451–454. Elsevier Science, New York, 1992.
[36] N. S. Brar, S. J. Bless and Z. Rosenberg. Impact induced failure waves in glass bars and plates. *Applied Physics Letters*, 59(26):3396–3398, 1991.
[37] N. S. Brar and S. J. Bless. Failure waves in glass under dynamic compression. *High Pressure Research*, 10(5-6):773–784, 1992.
[38] G. F. Raiser, J. L. Wise, R. J. Clifton, D. E. Grady and D. E. Cox. Plate impact response of ceramics and glasses. *Journal of Applied Physics*, 75(8):3862–3869, 1994.
[39] N. K. Bourne, Z. Rosenberg and J. E. Field. Plate impact response of ceramics and glasses. *Journal of Applied Physics*, 78(6):3736–3739, 1995.
[40] D. P. Dandekar and P. A. Beaulieu. Failure waves under shock wave compression in soda lime glass. In L. e. Murr, editor, *Metallurgical and Materials Applications of Shock-Wave and High-Strain-Rate Phenomenona*, Proceedings of the 1995 International Conference on Metallurgical and Materials Applications of Shock-Wave and High-Strain-Rate Phenomena (EXPLOMET '95), pages 211–218. Elsevier, Amsterdam, Oxford, 1995.
[41] S. Sundaram. *Pressure-Shear Plate Impact Studies of Alumina Ceramics and the Influence of an Intergranular Glassy Phase*. PhD thesis, Brown University, Providence, RI, May 1998.

[42] M. Ortiz, A. M. Cuitiño, J. Knap and M. Koslowski. Mixed atomistic-continuum models of material behavior: The art of transcending atomistics and informing continua. *MRS Bulletin*, 26(3):216–221, March 2001.

[1]Division of Engineering and Applied Science, California Institute of Technology, 1200 E. California Blvd., Pasadena, CA 91125, USA., [2]Institut de Recherche en Génie Civil et Mécanique (GeM - UMR 6183), École Centrale de Nantes, 1 rue de la Noë - BP 92101, 44321 Nantes cedex 3, France.

E-mail address: ortiz@caltech.edu

Dear editors:

Thank you for your consideration of the revision of our manuscript entitled: “Shear localization as a mesoscopic stress-relaxation mechanism in fused silica glass at high strain rates,” Ref: JMPS 2019 1006, co-authored with W. Schill, J.P. Mendez and L. Stainier. We are not aware of any conflicts of interest.

Sincerely,

Professor Michael Ortiz
Frank and Ora-Lee Marble Professor
of Aeronautics and Mechanical Engineering
California Institute of Technology
Mail Code 105-50
Pasadena, CA 91125
Phone: (626) 395-4530
Fax: (626) 395-1396
E-mail: ortiz@caltech.edu
http://www.ortiz.caltech.edu/

Dear editors:

We would appreciate your consideration of the revision of our manuscript entitled: “Shear localization as a mesoscopic stress-relaxation mechanism in fused silica glass at high strain rates,” Ref: JMPS 2019 1006, co-authored with W. Schill, J.P. Mendez and L. Stainier. We have addressed all the substantive queries raised by the referees and made the corresponding changes to the manuscript.

Sincerely,

Professor Michael Ortiz
Frank and Ora-Lee Marble Professor
of Aeronautics and Mechanical Engineering
California Institute of Technology
Mail Code 105-50
Pasadena, CA 91125
Phone: (626) 395-4530
Fax: (626) 395-1396
E-mail: ortiz@caltech.edu
http://www.ortiz.caltech.edu/